JGR Atmospheres

RESEARCH ARTICLE
10.1029/2023JD039761

Mountaintop Gamma Ray Observations of Three Terrestrial Gamma-Ray Flashes at the Säntis Tower, Switzerland With Coincident Radio Waveforms

Jeffrey M. Chaffin[1,2], David M. Smith[1], Jeff Lapierre[3], Steve Cummer[4], John Ortberg[1], Antonio Sunjerga[5], Amirhossein Mostajabi[5], Marcos Rubinstein[6], and Farhad Rachidi[5]

[1]University of California Santa Cruz, Santa Cruz, CA, USA, [2]Air Force Institute of Technology, WPAFB, Fairborn, OH, USA, [3]Earth Networks, Germantown, MD, USA, [4]Duke University, Durham, NC, USA, [5]Swiss Federal Institute of Technology (EPFL), Lausanne, Switzerland, [6]University of Applied Sciences of Western Switzerland (HES-SO), Yverdon-les-Bains, Switzerland

Key Points:

- First terrestrial gamma ray flashe (TGF) observations from a mountaintop
- First ground observation of a TGF associated with a "slow pulse" radio sferic
- Possible stepped leader X-rays preceding a double pulsed TGF

Correspondence to:

J. M. Chaffin,
jmchaffi@ucsc.edu

Citation:

Chaffin, J. M., Smith, D. M., Lapierre, J., Cummer, S., Ortberg, J., Sunjerga, A., et al. (2024). Mountaintop gamma ray observations of three terrestrial gamma-ray flashes at the Säntis Tower, Switzerland with coincident radio waveforms. *Journal of Geophysical Research: Atmospheres*, *129*, e2023JD039761. https://doi.org/10.1029/2023JD039761

Received 8 AUG 2023
Accepted 13 JAN 2024

Abstract We report on the mountain top observation of three terrestrial gamma-ray flashes (TGFs) that occurred during the summer storm season of 2021. To our knowledge, these are the first TGFs observed in a mountaintop environment and the first published European TGFs observed from the ground. A gamma-ray sensitive detector was located at the base of the Säntis Tower in Switzerland and observed three unique TGF events with coincident radio sferic data characteristic of TGFs seen from space. We will show an example of a "slow pulse" radio signature (Cummer et al., 2011, https://doi.org/10.1029/2011GL048099; Lu et al., 2011, https://doi.org/10.1029/2010JA016141; Pu et al., 2019, https://doi.org/10.1029/2019GL082743; Pu et al., 2020, https://doi.org/10.1029/2020GL089427), a −EIP (Lyu et al., 2016, https://doi.org/10.1002/2016GL070154; Lyu et al., 2021, https://doi.org/10.1029/2021GL093627; Wada et al., 2020, https://doi.org/10.1029/2019JD031730), and a double peak TGF associated with an extraordinarily powerful and complicated positive-polarity sferic, where each TGF peak is possibly preceded by a short burst of stepped leader emission.

Plain Language Summary We present the first report of mountain top observations of terrestrial gamma-ray flashes (TGFs) that occurred during the summer storm season of 2021. A gamma-ray sensitive detector was placed at the base of the Säntis Tower in Switzerland and detected three distinct TGF events. Each event is associated with a coincident lightning flash. We analyze the radio emission of the associated lightning flash and make comparisons with previously published associations between TGFs and certain radio sferics. Additionally, one of the observed TGFs is likely a two-pulse event where each gamma-ray peak may be preceded in time by a brief burst of X-ray stepped leader emission.

1. Introduction

Terrestrial gamma ray flashes (TGFs) are submillisecond bursts of radiation (up to 10s of MeV) generated in thunderstorms and closely associated with lightning (Briggs et al., 2010; Cummer et al., 2005; Fishman et al., 1994; Smith et al., 2005; Stanley et al., 2006). The source of the gamma ray production, via the bremsstrahlung mechanism, is understood to be an exponentially growing population of relativistic electrons or relativistic runaway electron avalanches (RREA) within the electric fields associated with the lightning leader process and possibly to an unknown extent the local ambient field (Dwyer, 2003; Dwyer et al., 2012; Gurevich et al., 1992; Lehtinen et al., 1996; Wilson, 1925). However, the mechanism of the TGF and its connection to lightning leader propagation is not fully understood. This has led to a recent focus on multi-wavelength observations which can shed light on the temporal relationship between TGFs and radio signatures of different lightning processes.

The last decade has seen some compelling multi-wavelength observations in lightning leader radio emission that have linked a subset of TGF satellite observations with two specific types of radio waveforms during lightning leader propagation. "Slow pulse" events (Cummer et al., 2011; Lu et al., 2011; Pu et al., 2019, 2020), observed in the midst of initial breakdown pulses (IBPs) of relatively small peak current lightning events, are characterized by a distinct slow temporal signature that matches the durration of the associated TGF and is near-simultaneous (within a few microseconds) with the mean of gamma ray arrival times. Dwyer and Cummer (2013) showed how this slow pulse can be interpreted as an observable current moment of the TGF electron avalanche process itself.

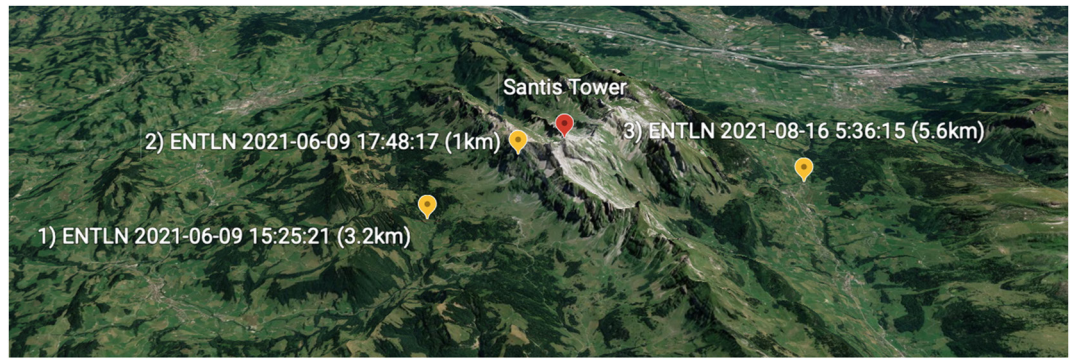

Figure 1. Earth Networks Total Lightning Network geo-locations (yellow markers) for each event and distance from the Säntis Tower (red marker).

The second kind of characteristic pulse, energetic in-cloud pulses (EIPs) (Cummer et al., 2017; Lyu et al., 2016, 2021), are high peak current sferics associated with negative leaders in positive intra-cloud (+IC) lightning. They are complicated and are longer in duration compared to narrow bipolar events, the other kind of powerful IC sferic. TGFs have been found to be time aligned (within about 10 μs) with +EIP sferics tens to hundreds of microseconds long (Cummer et al., 2011; Lu et al., 2011).

These distinct classes of sferics give a unique perspective into the behavior of the TGF mechanism not possible with gamma-ray observations alone. Although the observation of −EIPs and negative polarity slow pulses have been inferred to correspond with downward TGFs, thus far there have only been two published observations that directly make this connection, Pu et al. (2020) and Wada et al. (2020) which reported on a negative slow pulse and −EIP, respectively.

In addition to these two associations we report on the mountaintop observation of three TGF events, to our knowledge the first TGFs observed in a mountaintop environment. We will present multi-wavelength measurements making direct associations between two of the TGFs observed and low frequency (LF) radio sferic data of both a slow pulse event and a −EIP. A third TGF observation appears to be a double pulse event coincident with a very strong and complex high peak current radio sferic, and was close enough to the tower to observe the neutron afterglow (Bowers et al., 2017; Enoto et al., 2017; Wada et al., 2019a, 2019b).

2. Instrumentation

A gamma-ray sensitive detector consisting of a $5 \times 5''$ plastic scintillator mounted to a conventional photomultiplier (PMT) tube was located at the base of the Säntis Tower on Mt. Säntis, Switzerland at an elevation of 2.5 km. The average effective area of the plastic detector is 45 cm^2. The analog output of the PMT was routed to a Bridgeport Instruments eMorpho MCA. The MCA uses an 80 MHz ADC and provides a time-tagged photon event list mode with the integrated pulse area (with 16-bit resolution) and arrival time (with 32-bit/12.5 ns resolution). Earth Networks Total Lightning Network (ENTLN) provided geolocation of individual lightning flashes using an array of ground-based sensors located throughout the European continent using LF radio sferic data.

3. Measurement and Analysis

On the 9 June 2021 two TGFs were observed during a series of thunderstorm cells passing over Mt. Säntis. Event 1 was a roughly 150 μs duration flash of gamma photons coincident with a −IC (−10 kA) lightning leader at 15:25:21.165148 UTC with an ENTLN location of 3.2 km from the Säntis Tower. Event 2 was a double pulse gamma ray flash lasting 400 μs in total. This second event was coincident with a strong (100 kA) and unusually complex +IC sferic at 17:48:17.847036 UTC located 1 km from the Säntis Tower. Event 3 occurred on the 16 August 2021 coincident with a −135 kA lightning sferic at 5:38:15.3093 UTC and 5.6 km from the Säntis Tower. All three events and their distances relative to the Mt. Säntis Tower is displayed in Figure 1. Unfortunately, at the time of these observations the instrument computer clock was malfunctioning, and absolute timing can only be certain to 1–2 ms. This is sufficient to associate each event to a lightning flash but insufficient to say anything

quantitative regarding the timing relationship between the TGF observation and the leader progression with time alignment of the data alone.

3.1. Event 1

Event 1 is associated with an ENTLN radio sferic on 9 June 2021 at 15:25:21.165148 UTC and 3.2 km from the Tower. The gamma ray observation was roughly 150 μs in duration and produced 60 counts in the detector with an energy range of 100 keV to 9 MeV. Unfortunately, there was significant pileup in the detector electronics during the brightest portion of the TGF resulting in a loss of counts and systematically giving the few recorded counts during the brightest portion artificially large energies. The sferic shows a slow pulse signal with negative polarity. The same as that described in Pu et al. (2019) but of opposite polarity indicating the movement of negative charge downward.

The pulse comes in the midst of short (<10 μs) IBPs and is similar in duration to the gamma-ray signal. If this radio sferic slow pulse is a signature of the current moment of the RREA mechanism then the gamma ray duration should match the slow pulse duration. To determine this we follow the example of Pu et al. (2019) by attempting to fit the arrival time distribution of the gamma rays to a Gaussian under the assumption that the RREA current moment follows a normal distribution. The Earth Networks sensors have a frequency response that is proportional to the radiative far-field electric field which is proportional to the derivative of the source current dI/dt. Assuming that the current pulse created by the RREA mechanism is Gaussian, the first derivative of the gamma ray arrival time distribution should be comparable to the slow pulse in the Earth Networks sensor data.

Unfortunately as mentioned previously the gamma ray data are significantly piled up during the brightest portion of the TGF. This makes determining an arrival time distribution challenging. We rely on a combination of GEANT4 (Agostinelli et al., 2003; Allison et al., 2006, 2016) Monte Carlo simulations of TGFs and Python code written to simulate the behavior of the PMT output trace and how the Bridgeport electronics processes the trace into individual photon counts. We start with a distribution of photons that are the output of a relativistic electron avalanche model (REAM) simulation discussed in Dwyer (2003, 2007) and Dwyer and Smith (2005). The REAM photon distribution has a RREA energy spectrum characteristic of TGFs observed from space. The photons act as the input to our own Geant4 code which simulates their transport through a model of the atmosphere, U.S. Standard Atmosphere (1976), and finally through a mass model of our plastic scintillator to obtain a simulated energy spectrum in the detector which takes into account the detector material response.

Written in python, the electronics simulation software recreates the PMT output pulse of the instrument with the same rise and decay time characteristics. Given a specified number of interactions in the detector material and energy distribution of those interactions, the python code creates a pulse for each count with an amplitude scaled to the counts given energy and simulates "ADC samples" of the pulse every 12.5 ns. The pulses are than distributed according to a Gaussian arrival time distribution and the "ADC samples" of each pulse are added to a baseline array creating a facsimile of PMT trace data. The behavior of the instruments onboard FPGA is recreated in the python code to generate a list mode "photon by photon" data output from the simulated trace. This takes into account the pulse trigger threshold, integration window, dead time and pileup behavior.

We use the previously mentioned Geant4 derived detector response energy spectrum and adjust two parameters, the width of the Gaussian time distribution and the number of photon interactions in the detector until the list mode simulation output data matches the pile-up/dead time behavior, duration and number of counts in the TGF data. Figure 2 shows the TGF gamma ray energies versus time scatter plot in black and the simulated TGF with the electronics signal processing behavior accounted for in blue using a 42 μs FWHM time distribution and roughly 2,000 detector interactions. With an average effective area of 45 cm^2 the estimated fluence at the detector with 2,000 counts is 45 photons/cm^2. Though we don't know the actual altitude of the TGF we can estimate a range of source luminosity as a function of possible TGF altitudes with the known horizontal distance obtained from lightning LF sensor triangulation. For a given altitude we calculate the distance and "column density" in grammage of atmosphere (g/cm^2) between the TGF source and the instrument on Mt. Säntis. Assuming a downward 180° isotropic distribution and a TGF e-folding attenuation length of 45 g/cm^2 (Chaffin et al., 2023; Smith et al., 2010) the fluence at the instrument can be estimated for a given source luminosity. Figure 3 shows the luminosity (black curve) required at TGF source altitudes between 3.5 and 10.5 km for the fluence at the instrument to agree with our estimate of 45 photons/cm^2 for event 1. This source luminosity range between 10^{16} and more than 10^{18} photons >1 MeV is consistent with orbital TGF observations.

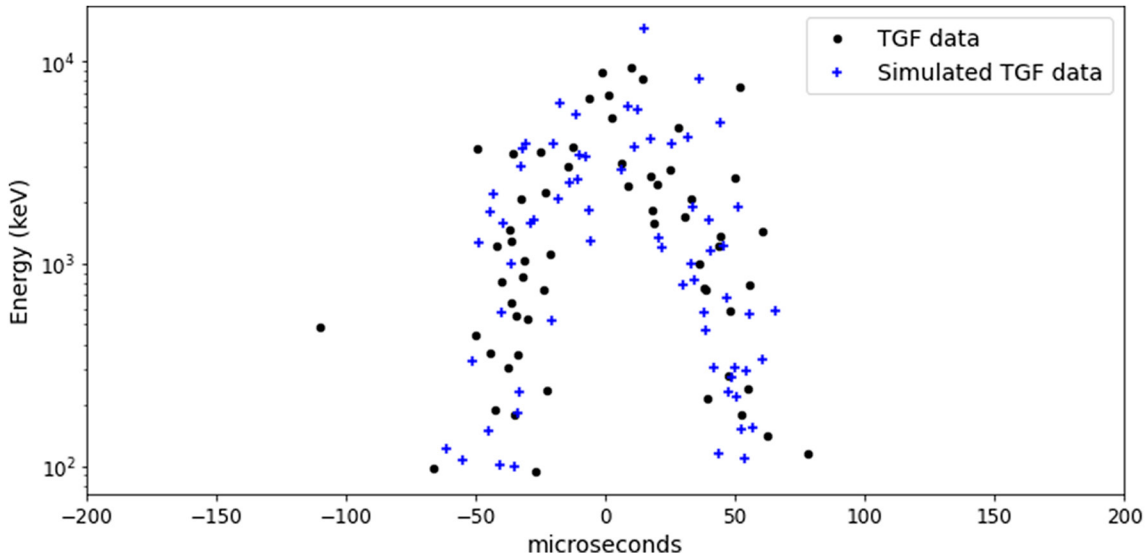

Figure 2. Gamma ray energies versus time. Black data points represent a single photon count. The limited number and lack of low energy counts in the middle of the signal is a result of pileup in the detector electronics. The high energy counts in the middle of the scatter plot are likely a sum of several lower energy photons. Blue data points represent simulated photon counts from an electronics response simulation code using a simulated terrestrial gamma ray flashe (TGF) with temporal distribution and number of photon interactions in the detector adjusted to match the dead time and pileup behavior of the real TGF data in black.

Figure 4 shows two plots that use a FWHM of 42 μs for the simulated TGF Gaussian and roughly 2,000 photon interactions in the detector. In the simulations (blue) 100 different TGFs with random energy and time samples of this Gaussian parent distribution were used to average the curves together. The real TGF data are in orange. The plot on the left is the average derived photon energy in each 5 μs bin, showing the effect of pileup. The plot on the right is the number of counts in each 5 μs bin, showing the duration and the effect of dead time. To the eye the 42 μs FWHM is a likely best fit with approximate errors of ±5 μs FWHM. In Figure 5 the first derivative of a 42 μs FWHM Gaussian is over plotted on the radio sferic slow pulse data and aligned in time with the simulated Gaussian count rate distribution. The first derivative of the Gaussian is in good agreement with the slow pulse confirming our assumption of a Gaussian source current derived from the gamma ray temporal distribution. Though the timing precision of the TGF observation isn't sufficient to time align the two data sets, the agreement between the sferic slow pulse and the first derivative of the Gaussian arrival time distribution along with the

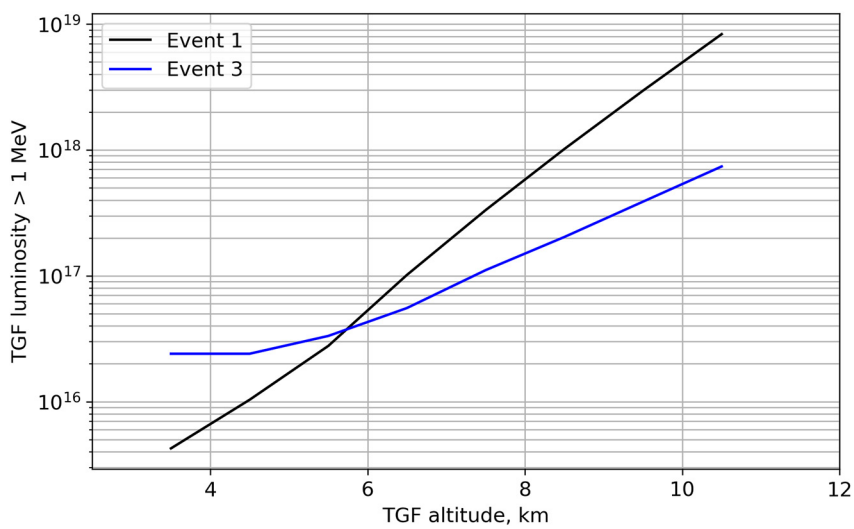

Figure 3. Intrinsic luminosity of terrestrial gamma ray flashe (TGF) for photons >1 MeV as a function of TGF altitude. Black curve represents Event 1 and the blue curve represents Event 3.

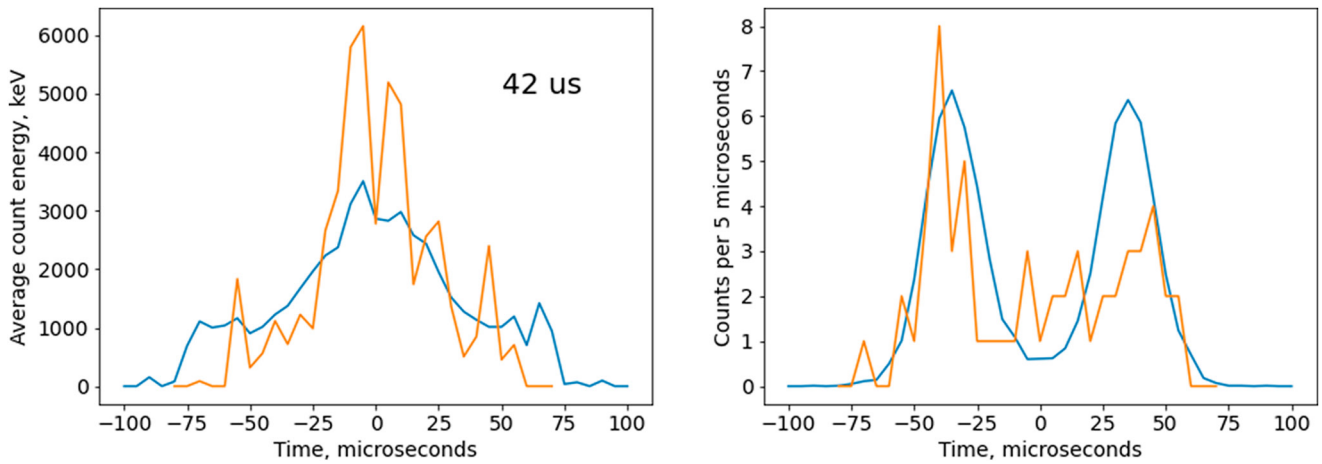

Figure 4. Left: average derived photon energy in each 5-μs bin; simulations in blue and terrestrial gamma ray flashe (TGF) data in orange. Right: number of counts in each 5-μs bin; simulations in blue and TGF data in orange.

work done by Pu et al. (2019, 2020) is compelling evidence that this slow pulse and gamma ray observation are the result of the same physical mechanism, making this the first ground based TGF observation linked to a slow pulse sferic.

3.2. Event 3

Event 3 took place on 16 August 2021. It was associated with an ENTLN sferic at 5:38:15.3093 UTC that was located 5.6 km from the Säntis Tower. At that distance from the source the gamma ray observation (Figure 6 bottom) doesn't appear to suffer from pileup or deadtime but is outside the detection radius of any neutron signal. The instrument recorded 28 counts from which we calculate a fluence of 0.62 photons/cm^2. Using the same analysis described in Section 3.1 a range of source luminosity is estimated as a function of TGF source altitude and plotted (blue curve) in Figure 3. Again, the order of magnitude of possible TGF luminosity of Event 3 is consistent with orbital TGF observations. The associated radio sferic (Figure 6 top) was a very high peak current (−135 kA) −IC event. With the exceptionally large peak current, big clear pulse in the LF radio data, and clear

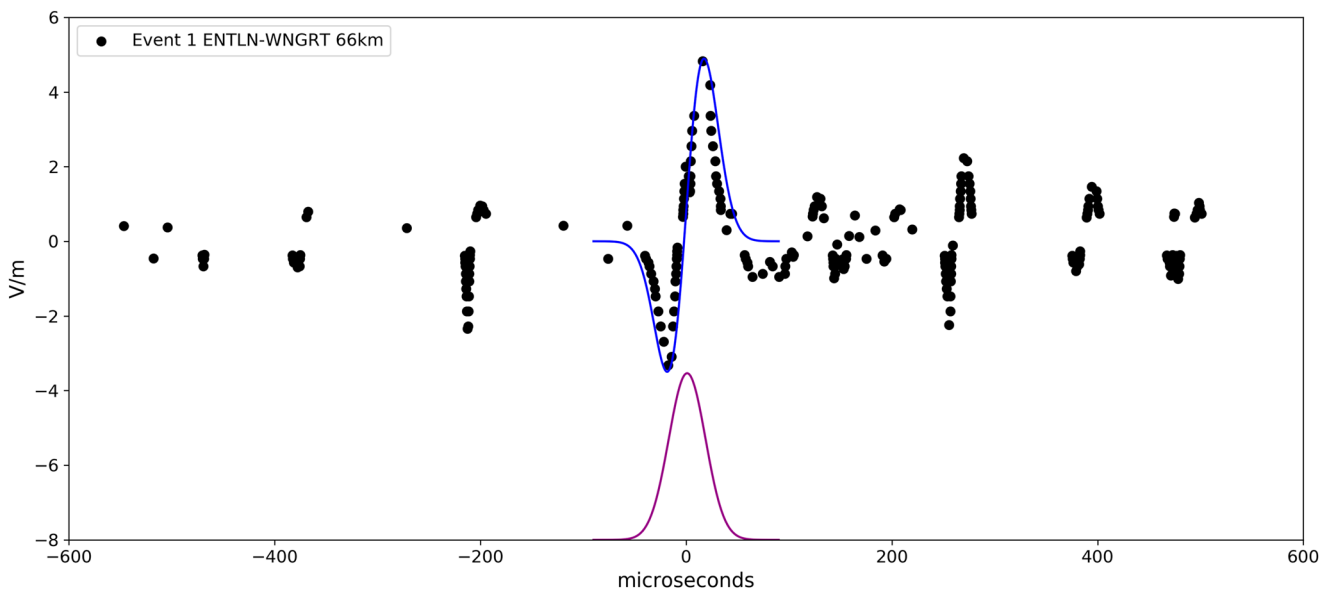

Figure 5. Event 1 radio sferic (black) of a −IC flash of −10 kA peak current. The first derivative (blue) of a 42 μs FWHM Gaussian (purple) is fit to the slow pulse portion of the sferic. The low frequency sensor was 66 km from the Säntis Tower.

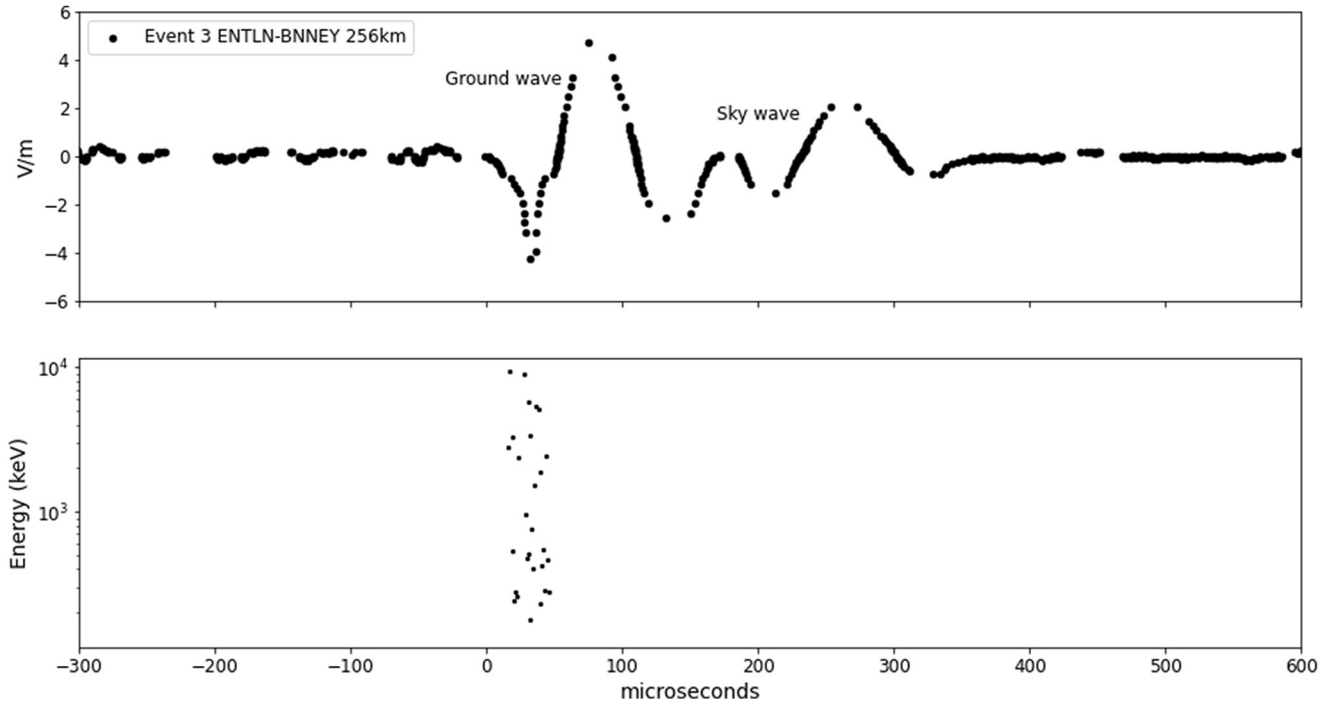

Figure 6. Top: Event 3 radio sferic of a −IC flash with 135 kA peak current. The flash was located 5.6 km from the Säntis Tower. The radio data is from an low frequency sensor 256 km from the flash. Bottom: terrestrial gamma ray flashe counts plotted by energy versus time. Note that the timing alignment between the radio sferic and gamma ray data is purely speculative. We have aligned the 50 μs of gamma ray counts with the initial 50 μs of the ground wave.

negative polarity we immediately suspected this to be a −EIP. To confirm this we sought to compare a known EIP to the waveform associated with our gamma ray signal.

When comparing LF waveforms it is crucial to make sure the comparisons are being made using sensors that were an equal distance to the source of the signal. The reason for this is related to the propagation times of both the ground wave and the sky wave. The closer the LF sensor is to the signal source the greater the time difference between the arrival of each at the sensor. For instance, you can see in the top plot of Figure 6 the radio sferic of Event 3 as recorded by a sensor 256 km from the source. You can clearly differentiate the ground wave signal lasting roughly 100 μs followed closely by the ionospheric reflection or sky wave.

In contrast, the radio sferic of Event 3 plotted in Figure 7 is from a sensor 425 km from the source signal. The ground wave and its reflection are too close together to differentiate making the signal appear quite different. From a collection of unpublished EIPs confirmed by both Duke University sensors and Earth Networks we found

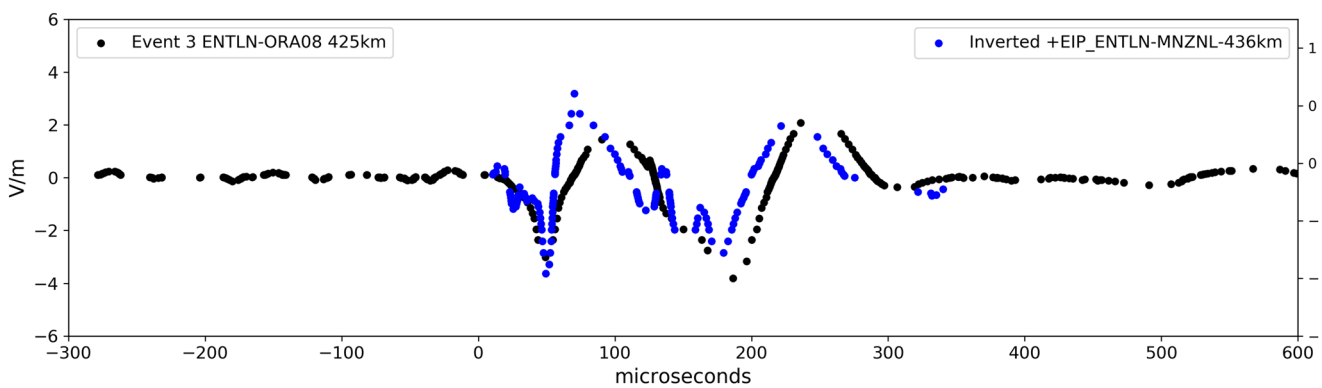

Figure 7. Event 3 radio sferic (black) using radio data from an low frequency sensor 425 km from the current source. Known +energetic in-cloud pulse (EIP) (blue) from an Earth Networks Total Lightning Network sensor 436 km from its current source. The known +EIP data have been inverted and over plotted onto the Event 3 waveform for comparison.

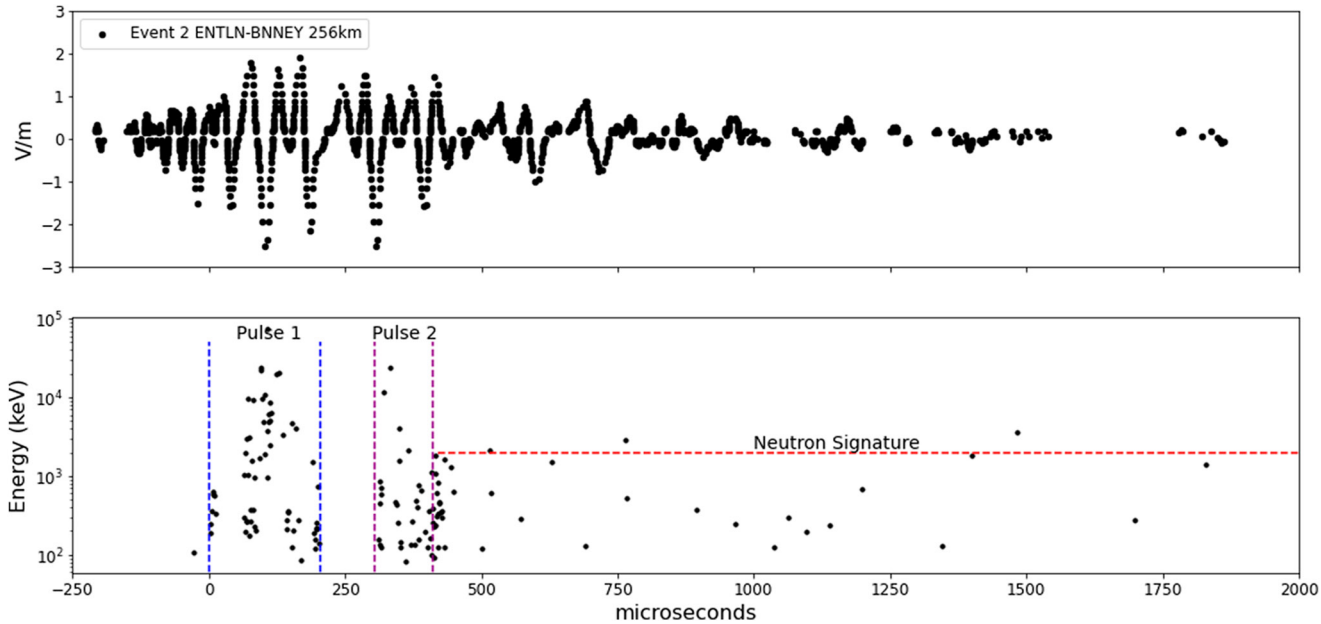

Figure 8. Top: Event 2 radio sferic of an +IC flash with 100 kA peak current. The flash was located 1 km from the Säntis Tower. The radio data is from an Earth Networks Total Lightning Network low frequency sensor 256 km from the flash. Bottom: terrestrial gamma ray flashe counts plotted by energy versus time. Possible double pulse event with a neutron afterglow starting at 400 μs. Note that the timing alignment between the radio sferic and gamma ray data is purely speculative. We have aligned the 400 μs of gamma ray counts with the 400 μs duration of the large peak amplitude and wide pulse width radio data.

a +EIP observation from a sensor 436 km from the signal source. We inverted the polarity of the known +EIP data and over plotted it on the Event 3 sferic from the 425 km distant sensor shown in Figure 7. The signals are remarkably similar except for the polarity inversion of the known EIP which indicates the source currents are also similar. We believe that the Säntis signal is consistent with a −EIP produced during a descending negative leader or upward propagating positive leader.

3.3. Event 2

We have saved Event 2 for last as it is a more complicated gamma ray observation and sferic. ENTLN recorded a large amplitude (100 kA) +IC radio sferic on the 9 June 2021 at 17:48:17.847036 UTC. The ENTLN location puts the lightning flash 1 km from the Säntis Tower. The radio waveform (Figure 8 top plot) is atypical of an IC radio sferic. It has an unusually high number of large amplitude pulses. The pulse durations of 100–150 μs are much longer than normal IBPs and the spacing of the largest-amplitude features matches the spacing of the TGF pulses as shown by the speculative alignment with the gamma ray data in Figure 8. The ENTLN sensor was only 256 km from the lightning location. At that distance the ground wave signal will dominate the associated sky wave. This suggests that the equally large amplitude pulses in this sferic represent distinct current pulses in the lightning event.

This was an extraordinarily powerful sferic compared to other flashes in the local environment. Figure 9 depicts the 14 highest peak current events identified as +IC by the European Cooperation for Lightning Detection in the prior year (2020) within 30 km of the Säntis Tower out of a total database of 4,598 +ICs in that distance range. The sferic data are from the same ENTLN sensor as our TGF-associated sferic shown in red at the bottom, and the distances between the current source and sensor vary between 245 and 291 km. Qualitatively, it is quite obvious how distinct the TGF associated trace is compared to the sample of high peak current traces in proximity to the Säntis Tower.

In order to quantify the uniqueness of this sferic we calculated the sum of the square of the E-field values, a measure of total radiated energy, that were recorded for each trace and plotted those values against each trace's peak current as shown in Figure 10. The peak current is calculated by ENTLN from the single largest amplitude pulse (E-field measurement data point) in a trace. The TGF-associated event has a $\sum E^2$ that is five times as large as its nearest competitor while the rest are clustered together. This does a nice job of capturing the unusualness

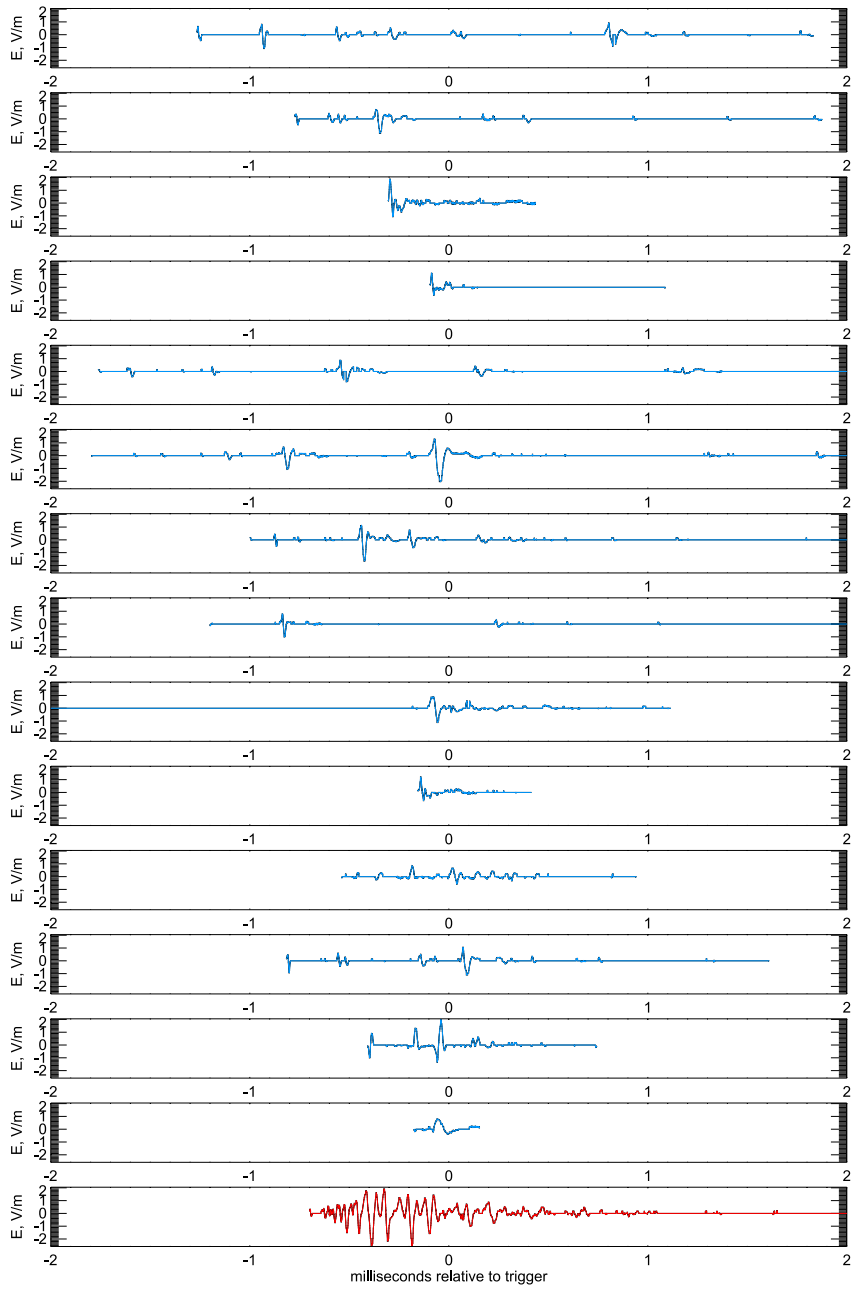

Figure 9. Earth Networks Total Lightning Network (ENTLN) radio data of the 14 largest peak current lightning events, within 30 km of the Säntis Tower from October 2019 to April 2021, and the Event 2 waveform in red. All traces are from the same ENTLN sensor at similar distances from the current source.

of the event. Not just that it reaches a high peak current, and not just that it has many pulses, but that it has many pulses at an equally high peak current.

From the gamma ray data (see Figure 8 bottom plot) the TGF appears to be a two peak event, but with significant pile-up and possible periods of detector paralysis. The trailing counts post-TGF of about 1.5 ms in duration indicate a neutron signature. Downward TGFs during winter thunderstorms in Japan have been shown to produce a number of neutrons via photonuclear reactions in the atmosphere (Bowers et al., 2017; Enoto et al., 2017; Wada et al., 2019a, 2019b). The thermalized neutrons with time scales on the order of milliseconds (Babich et al., 2007) interact in our plastic detector material and undergo neutron capture with hydrogen resulting in the hydrogen isotope deuterium in an excited state. The excited deuterium immediately relaxes to its ground state emitting a

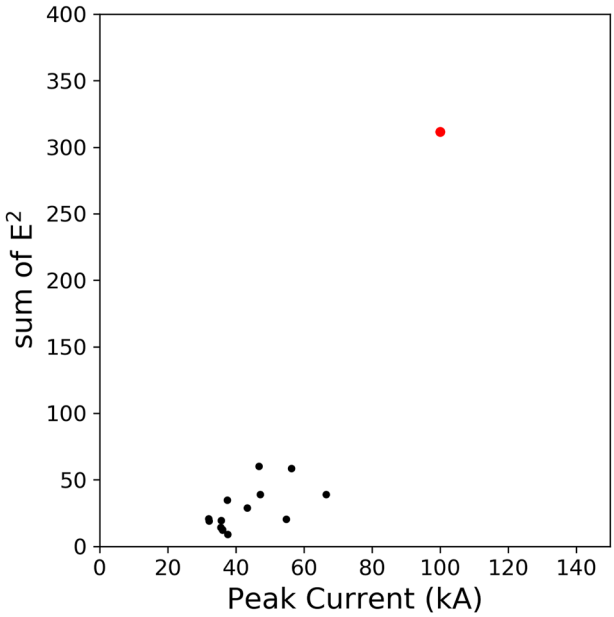

Figure 10. Sum of the square of the Earth Networks Total Lightning Network electric field data for each trace in Figure 9 plotted with respect to each event's peak current. The 14 highest peak current events are plotted in black and roughly clustered in the same region of the plot, whereas the Event 2 trace is plotted in red.

2.2 MeV gamma in our detector. The 2.2 MeV gamma deposits only a portion of its energy via Compton scattering before leaving the detector material resulting in a Compton shoulder at roughly 2 MeV. The background count rate of the instrument is roughly 500 counts/second which is equivalent to a count every 2 ms. During the 1.5 ms after the TGF the count rate exceeds the background expectation by a factor of 20 and the counts also appear to indicate a 2 MeV Compton shoulder.

We offer an alternative analysis of the gamma-ray arrival time data in Figure 8. Figure 11 shows roughly 400 μs of the double pulse TGF. It is possible that there are actually four distinct signals. The first signal is a short-duration burst of apparent low-energy counts. This burst could be stepped leader emission that precedes the initial TGF by about 60 μs. The TGF is about 150 μs in duration and the data exhibit detector paralysis and pulse pileup behavior, a period of no low-energy counts (not real), as the count rate increased. As we begin to see lower energy counts again, we assume that the count rate is decreasing. This is followed by a 20 μs gap before a second short burst of low-energy photons (stepped leader emission?) that precedes the second TGF pulse by 120 μs. If these isolated low energy counts are indeed stepped leader X-ray bursts their parent energy distribution would be inconsistent with an RREA energy spectrum and should exhibit a softer or lower average energy. To test this hypothesis we compare the average energy of the two possible X-ray burst counts to the average energies of 1 million equivalent sized samples of an RREA energy spectrum convolved with the detector response as shown in Figure 12. The RREA spectrum is rejected with a confidence of 98.58% for both bursts 1 and 2. This indicates that the parent distribution of the "X-ray bursts" may be softer and thus inconsistent with RREA. To definitively say if the gaps between these signals and the two main pulses are real or merely periods of instrument dead-time due to extremely high count rates, the ADC sampled output of the PMT would need to be analyzed. Unfortunately, the instrument does not have the capability to save PMT trace data. Lacking data to confirm instrument behavior, this interpretation remains speculative, but possibly very important.

A possible explanation for the unusualness of the Event 2 waveform may be directly connected to the multi-pulse TGF observation just described. Could this be a multi-pulse +EIP? We know Event 3 to be an example of a

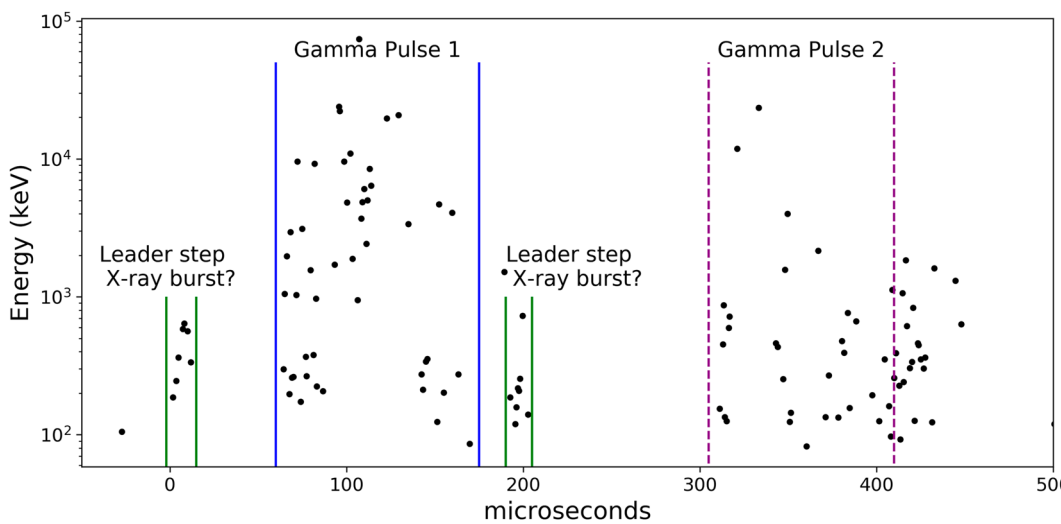

Figure 11. Event 2 double pulse terrestrial gamma ray flashe (TGF) listmode gamma ray data. Speculative interpretation of four separate X- and gamma-ray emissions within the 400 μs duration of the event. Two possible stepped leader bursts each preceding one of the two TGFs.

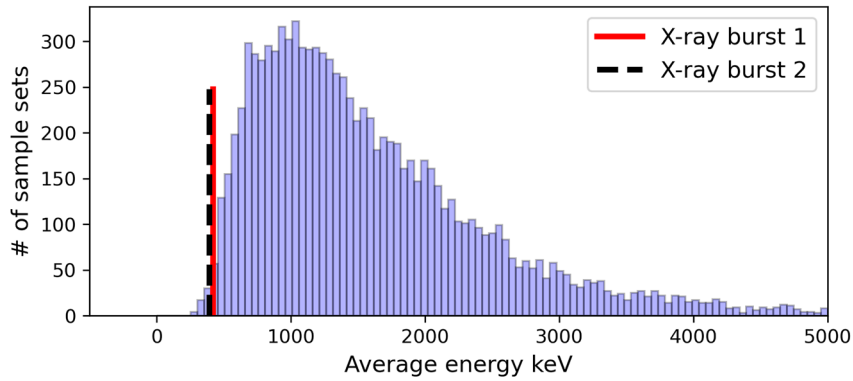

Figure 12. Blue: Histogram of the average energy of 1 million sample sets (sample size 7) of an relativistic runaway electron avalanches (RREA) energy distribution. Red line: Denotes the average energy of the first possible X-ray burst. Black dashed line: Denotes the average energy of the second possible X-ray burst. The RREA spectrum is rejected with a confidence of 98.58% for bursts 1 and 2.

confirmed −EIP observed by the same radio sensor as Event 2 and from an equivalent distance from the source. We compare the Event 2 waveform to the Event 3 −EIP by inverting the Event 3 sferic and summing two versions of the inverted data but separated in time. In Figure 13 the green dashed lines are separated by 210 μs. This appears to be the time separation between the most piledup/paralyzed moments in each TGF pulse. This comes earlier for the second pulse, which is why it is shorter than the delay between the starts of the pulses. Top panel is Event 3 inverted. Middle panel has two "Event 3s" spaced by 210 μs and summed. The bottom panel is Event 2. It is of course speculative but the behavior appears to have similarities and may explain Event 2's multiple pulses at equally high peak current.

The final enigma of Event 2 is its clear positive polarity. The ENTLN sensors classified this lightning event as being a +IC, which describes an intra-cloud leader channel moving negative charge upward. Depending on the source altitude of the TGF, which is unknown, this could be a reverse beam observation from the ground as first modeled in Ortberg et al. (2020). It is also possible that the event was lateral to or lower in altitude with respect to the observation point (2.5 km) making the main beam visible to the tower and instrument. A detailed meteorological analysis of the storm and its possible charge structure and altitudes would need to be done to begin to answer this question.

4. Conclusion

The vast majority of TGFs have been detected by spaced-based instruments (Briggs et al., 2010; Fishman et al., 1994; Marisaldi et al., 2010; Neubert et al., 2020; Østgaard et al., 2019; Smith et al., 2005) and are dominated by associations with positive IC lightning leaders. TGFs however have turned out to be linked to a wide variety of lightning types and atmospheric conditions, as evidenced by these unique Mt. Säntis events and the numerous ground based observations of downward directed TGFs (Abbasi et al., 2022; Bowers et al., 2017; Colalillo, 2017; Dwyer & Cummer, 2013; Dwyer et al., 2003, 2004a, 2004b; Enoto et al., 2017; Hare et al., 2016; Smith et al., 2018; Tran et al., 2015; Wada et al., 2022). As challenging as ground observations are, the potential to observe the finer details of the relationship between the gamma ray fluence and the lightning leader current fluctuations cannot be overstated. Though orbital observations have provided large data sets and continue to contribute to our understanding of the TGF mechanism there are clear advantages to observations made within a few km of the TGF source. They include the ability to observe the varied particle physics associated with TGFs such as photo-neutrons (Bowers et al., 2017), positrons, and certain radioactive decay elements (Enoto et al., 2017). As speculated in this paper it may also be possible to observe stepped leader emissions that precede and are possibly integral to the TGF mechanism.

A further possibility of ground or airborne observations is obtaining photon arrival time distributions unaffected by the 100s of km of atmospheric transport between storm cloud altitudes and orbital spacecraft with sufficient numbers of counts to be statistically robust. These in situ observations could help determine whether there is an underlying behavior of discrete bursts of emission in the overall TGF time profile. As of November 2021

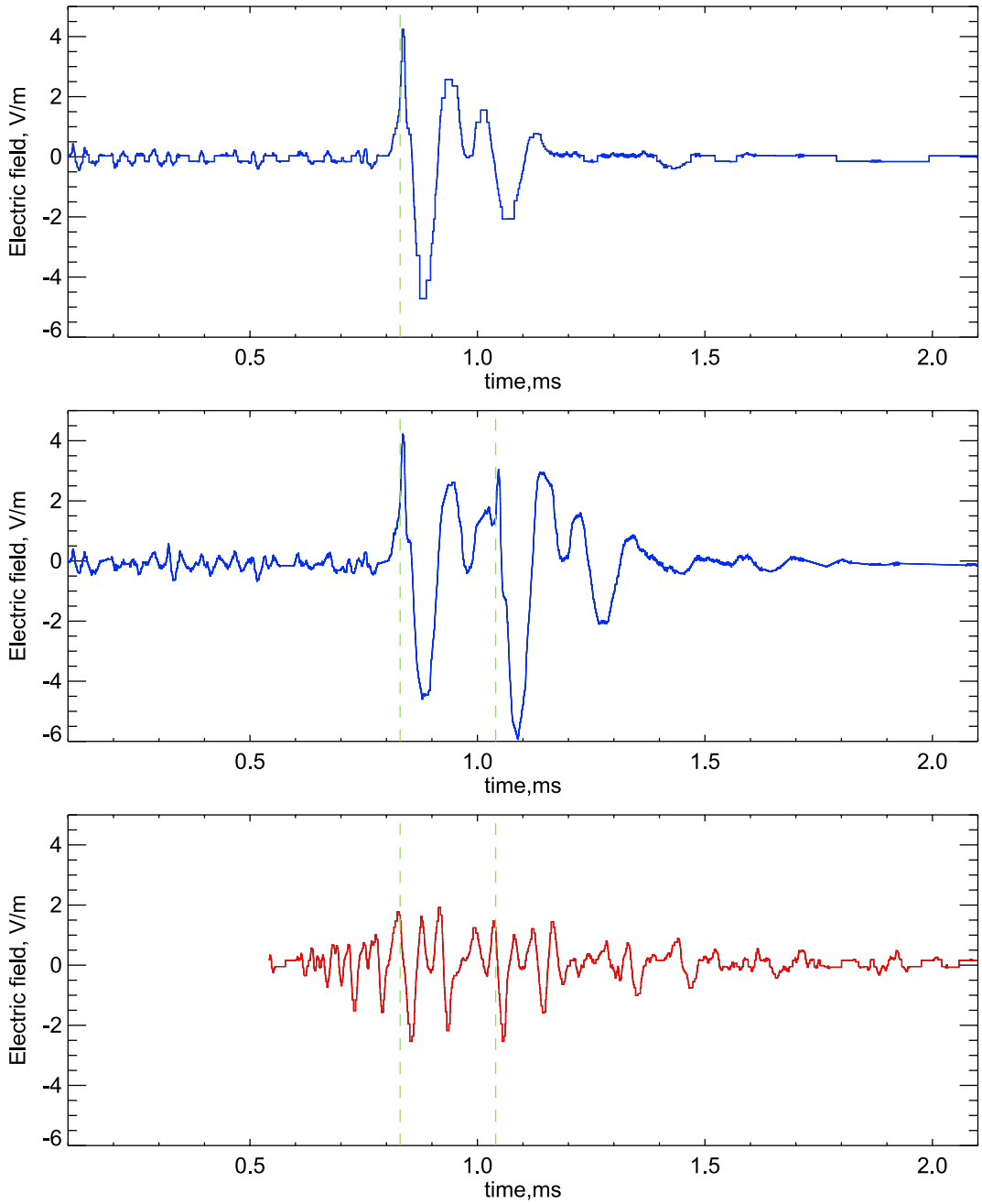

Figure 13. Top: Event 3 waveform inverted. Middle: Two inverted Event 3 waveforms separated by 210 μs and summed. Bottom: Event 2 waveform.

one of the six THOR instruments developed by the high energy atmospheric physics group at the University of California Santa Cruz has been deployed to the base of the Säntis Tower and the other five have been deployed elsewhere around the globe including Japan, New Mexico and Florida. We hope that over the next few years the observations made by these instruments, along with radio sferic data, will contribute to a greater understanding of the lightning-TGF relationship.

Data Availability Statement

The data files used in this work are available at Chaffin (2023).

Acknowledgments
J. M. C. and D. M. S. acknowledge the support of the National Science Foundation Award AGS-2235299.

References

Abbasi, R. U., Belz, J. W., Saba, M. M. F., Krehbiel, P. R., Remington, J., Stanley, M. A., et al. (2022). First high-speed camera observations of the optical counterpart of a terrestrial gamma-ray flash. eprint arXiv:2205.05115.

Agostinelli, A., Amako, A., Araujo, A., Apostolakis, J., Araujo, H., Arce, P., et al. (2003). Geant4 - A simulation toolkit. *Nuclear Instruments and Methods in Physics Research*, *506*(3), 250–303. https://doi.org/10.1016/S0168-9002(03)01368-8

Allison, A., Apostolakis, A., Asai, A., Arce, P., Asai, M., Aso, T., et al. (2016). Recent developments in GEANT4. *Nuclear Instruments and Methods in Physics Research*, *835*, 186–225. https://doi.org/10.1016/j.nima.2016.06.125

Allison, A., Apostolakis, A., Dubois, A., Araujo, H., Arce Dubois, P., Asai, M., et al. (2006). GEANT4 developments and applications. *IEEE Transactions on Nuclear Science*, *53*(1), 270–278. https://doi.org/10.1109/TNS.2006.869826

Babich, L. P., Kudryavtsev, A. Y., Kudryavtseva, M. L., & Kutsyk, I. M. (2007). Terrestrial gamma-ray flashes and neutron pulses from direct simulations of gigantic upward atmospheric discharge. *Soviet Journal of Experimental and Theoretical Physics Letters*, *85*(10), 483–487. https://doi.org/10.1134/S0021364007100037

Bowers, G. S., Smith, D. M., Martinez-McKinney, G. F., Kamogawa, M., Cummer, S. A., Dwyer, J. R., et al. (2017). Gamma ray signatures of neutrons from a terrestrial gamma ray flash. *Geophysical Research Letters*, *44*(19), 10. https://doi.org/10.1002/2017GL075071

Briggs, M. S., Fishman, G. J., Connaughton, V., Bhat, P. N., Paciesas, W. S., Preece, R. D., et al. (2010). First results on terrestrial gamma ray flashes from the Fermi Gamma-ray burst monitor. *Journal of Geophysical Research*, *115*(A7), A07323. https://doi.org/10.1029/2009JA015242

Chaffin, J. M. (2023). Mountaintop gamma ray observations of three terrestrial gamma-ray flashes at the Säntis tower, Switzerland with coincident radio waveforms [Dataset]. Dryad. https://doi.org/10.5061/dryad.r2280gbjf

Chaffin, J. M., Pu, Y., Smith, D. M., Cummer, S., & Splitt, M. (2023). Determining a lower limit of luminosity for the first satellite observation of a reverse beam terrestrial gamma ray flash associated with a cloud to ground lightning leader. *Journal of Geophysical Research: Atmospheres*, *128*(18), e2023JD038885. https://doi.org/10.1029/2023JD038885

Colalillo, R. (2017). Peculiar lightning-related events observed by the surface detector of the Pierre Auger Observatory. In *Proceedings of 35th international cosmic ray conference — PoS(ICRC2017)*. https://doi.org/10.22323/1.301.0314

Cummer, S. A., Lu, G., Briggs, M. S., Connaughton, V., Xiong, S., Fishman, G. J., & Dwyer, J. R. (2011). The lightning-TGF relationship on microsecond timescales. *Geophysical Research Letters*, *38*(14), 14810. https://doi.org/10.1029/2011GL048099

Cummer, S. A., Lyu, F., Briggs, M. S., Cramer, E., Stanbro, M., Roberts, O., & Smith, D. M. (2017). The connection between terrestrial gamma-ray flashes and energetic in-cloud lightning pulses. In *AGU 2017 Fall Meeting*.

Cummer, S. A., Zhai, Y., Hu, W., Smith, D. M., Lopez, L. I., & Stanley, M. A. (2005). Measurement and implications of the relationship between lightning and terrestrial gamma-ray flashes. *Geophysical Research Letters*, *32*(8), L22804. https://doi.org/10.1029/2005gl022778

Dwyer, J. R., Smith, D., & Cummer, S. (2012). High−Energy atmospheric physics: Terrestrial gamma-ray flashes and related phenomena. *Space Science Reviews*, *173*(1–4), 133–196. https://doi.org/10.1007/s11214-012-9894-0

Dwyer, J. R. (2003). A fundamental limit on electric fields in air. *Geophysical Research Letters*, *30*(20), 2055. https://doi.org/10.1029/2003gl017781

Dwyer, J. R. (2007). Relativistic breakdown in planetary atmospheres. *Physics of Plasmas*, *14*(4), 042901. https://doi.org/10.1063/1.2709652

Dwyer, J. R., & Cummer, S. A. (2013). Radio emissions from terrestrial gamma-ray flashes. *Journal of Geophysical Research: Space Physics*, *118*(6), 3769–3790. https://doi.org/10.1002/jgra.50188

Dwyer, J. R., Rassoul, H., Al-Dayeh, M., Caraway, L., Chrest, A., Wright, B., et al. (2004a). A ground level gamma-ray burst observed in association with rocket-triggered lightning. *Geophysical Research Letters*, *31*(5), L05119. https://doi.org/10.1029/2003GL018771

Dwyer, J. R., Rassoul, H., Al-Dayeh, M., Caraway, L., Chrest, A., Wright, B., et al. (2004b). Measurements of x-ray emission from rocket-triggered lightning. *Geophysical Research Letters*, *31*(5), L05118. https://doi.org/10.1029/2003GL018770

Dwyer, J. R., & Smith, D. M. (2005). A comparison between Monte Carlo simulations of runaway breakdown and terrestrial gamma-ray flash observations. *Geophysical Research Letters*, *32*(22), L08811. https://doi.org/10.1028/2005GL023848

Dwyer, J. R., Uman, M. A., Rassoul, H. K., Al-Dayeh, M., Caraway, L., Jerauld, J., et al. (2003). Energetic radiation produced during rocket-triggered lightning. *Science*, *299*(5607), 694–697. https://doi.org/10.1126/science.1078940

Enoto, T., Wada, Y., Furuta, Y., Nakazawa, K., Yuasa, T., Okuda, K., et al. (2017). Photonuclear reactions triggered by lightning discharge. *Nature*, *551*(7681), 481–484. https://doi.org/10.1038/nature24630

Fishman, G. J., Bhat, P. N., Mallozzi, R., Horack, J. M., Koshut, T., Kouveliotou, C., et al. (1994). Discovery of intense gamma-ray flashes of atmospheric origin. *Science*, *264*(5163), 1313–1316. https://doi.org/10.1126/science.264.5163.1313

Gurevich, A., Milikh, G. M., & Roussel-Dupré, R. A. (1992). Runaway electron mechanism of air breakdown and preconditioning during a thunderstorm. *Physics Letters A*, *165*(5–6), 463–468. https://doi.org/10.1016/0375-9601(92)90348-p

Hare, B. M., Uman, M. A., Dwyer, J. R., Jordan, D. M., Biggerstaff, M. I., Caicedo, J. A., et al. (2016). Ground-level observation of a terrestrial gamma ray flash initiated by a triggered lightning. *Journal of Geophysical Research: Atmospheres*, *121*(11), 6511–6533. https://doi.org/10.1002/2015JD024426

Lehtinen, N., Walt, M., Inan, U., Bell, T., & Pasko, V. (1996). γ-ray emission produced by a relativistic beam of runaway electrons accelerated by quasi-electrostatic thundercloud fields. *Geophysical Research Letters*, *23*(19), 2645–2648. https://doi.org/10.1029/96gl02573

Lu, G., Cummer, S. A., Li, J., Han, F., Smith, D. M., & Grefenstette, B. W. (2011). Characteristics of broadband lightning emissions associated with terrestrial gamma ray flashes. *Journal of Geophysical Research*, *116*(A15), A03316. https://doi.org/10.1029/2010JA016141

Lyu, F., Cummer, S. A., Briggs, M., Marisaldi, M., Blakeslee, R. J., Bruning, E., et al. (2016). Ground detection of terrestrial gamma ray flashes from distant radio signals. *Geophysical Research Letters*, *43*(16), 8728–8734. https://doi.org/10.1002/2016GL070154

Lyu, F., Cummer, S. A., Briggs, M., Smith, D. M., Mailyan, B., & Lesage, S. (2021). Terrestrial gamma-ray flashes can be detected with radio measurements of energetic in-cloud pulses during thunderstorms. *Geophysical Research Letters*, *48*(11), e2021GL093627. https://doi.org/10.1029/2021GL093627

Marisaldi, M., Fuschino, F., Labanti, C., Galli, M., Longo, F., Del Monte, E., et al. (2010). Detection of terrestrial gamma ray flashes up to 40 MeV by the AGILE satellite. *Journal of Geophysical Research*, *115*(A3), A00E13. https://doi.org/10.1029/2009JA014502

Neubert, T., Østgaard, N., Reglero, V., Chanrion, O., Heumesser, M., Dimitriadou, K., et al. (2020). A terrestrial gamma-ray flash and ionospheric ultraviolet emissions powered by lightning. *Science*, *367*(6474), 183–186. https://doi.org/10.1126/science.aax3872

Ortberg, J., Smith, D. M., Li, J., Dwyer, J., & Bowers, G. (2020). Detecting an upward terrestrial gamma ray flash from its reverse positron beam. *Journal of Geophysical Research: Atmospheres*, *125*(6), e2019JD030942. https://doi.org/10.1029/2019JD030942

Østgaard, N., Balling, J. E., Bjørnsen, T., Brauer, P., Budtz-Jørgensen, C., Bujwan, W., et al. (2019). The modular x- and 1 gamma-ray sensor (MXGS) of the ASIM payload on the international space station. *Space Science Reviews*, *215*, 1–28. https://doi.org/10.1007/s11214-018-0573-7

Pu, Y., Cummer, S. A., Huang, A., Briggs, M., Mailyan, B., & Lesage, S. (2020). A satellite-detected terrestrial gamma ray flash produced by a cloud-to-ground lightning leader. *Geophysical Research Letters*, *47*(15), e2020GL089427. https://doi.org/10.1029/2020GL089427

Pu, Y., Cummer, S. A., Lyu, F., Briggs, M., Mailyan, B., Stanbro, M., & Roberts, O. (2019). Low frequency radio pulses produced by terrestrial gamma-ray flashes. *Geophysical Research Letters*, *46*(12), 6990–6997. https://doi.org/10.1029/2019GL082743

Smith, D. M., Bowers, G. S., Kamogawa, M., Wang, D., Ushio, T., Ortberg, J., et al. (2018). Characterizing upward lightning with and without a terrestrial gamma ray flash. *Journal of Geophysical Research: Atmospheres*, *123*(20), 11321–11332. https://doi.org/10.1029/2018jd029105

Smith, D. M., Hazelton, B. J., Grefenstette, B. W., Dwyer, J. R., Holzworth, R. J., & Lay, E. H. (2010). Terrestrial gamma ray flashes correlated to storm phase and tropopause height. *Journal of Geophysical Research*, *115*(A8), A00E49. https://doi.org/10.1029/2009JA014853

Smith, D. M., Lopez, L. I., Lin, R. P., & Barrington-Leigh, C. P. (2005). Terrestrial gamma-ray flashes observed up to 20 MeV. *Science*, *307*(5712), 1085–1088. https://doi.org/10.1126/science.1107466

Stanley, M. A., Shao, X., Smith, D. M., Lopez, L., Pongratz, M., Harlin, J., et al. (2006). A link between terrestrial gamma-ray flashes and intracloud lightning discharges. *Geophysical Research Letters*, *33*(6), L06803. https://doi.org/10.1029/20005GL025537

Tran, M., Rakov, V., Mallick, S., Dwyer, J., Nag, A., & Heckman, S. (2015). A terrestrial gamma-ray flash recorded at the Lightning Observatory in Gainesville, Florida. *Journal of Atmospheric and Solar-Terrestrial Physics*, *136*, 86–93. https://doi.org/10.1016/j.jastp.2015.10.010

Wada, Y., Enoto, T., Nakazawa, K., Furuta, Y., Yuasa, T., Nakamura, Y., et al. (2019a). Downward terrestrial gamma-ray flash observed in a winter thunderstorm. *Physical Review Letters*, *123*(6), 061103. https://doi.org/10.1103/physrevlett.123.061103

Wada, Y., Enoto, T., Nakamura, Y., Furuta, Y., Yuasa, T., Nakazawa, K., et al. (2019b). Gamma-ray glow preceding downward terrestrial gamma-ray flash. *Nature, Communications Physics*, *2*(1), 67. https://doi.org/10.1038/s42005-019-0168-y

Wada, Y., Enoto, T., Nakamura, Y., Morimoto, T., Sato, M., Ushio, T., et al. (2020). High peak-current lightning discharges associated with downward terrestrial gamma-ray flashes. *Geophysical Research Letters*, *125*(4), e2019JD031730. https://doi.org/10.1029/2019JD031730

Wada, Y., Morimoto, T., Nakamura, Y., Wu, T., Enoto, T., Nakazawa, K., et al. (2022). Characteristics of low-frequency pulses associated with downward terrestrial gamma-ray flashes. *Geophysical Research Letters*, *49*(5), e2021GL097348. https://doi.org/10.1029/2021GL097348

Wilson, C. T. R. (1925). The electric field of a thundercloud and some of its effects. *Proceedings of the Physical Society of London*, *37*, 32D. https://doi.org/10.1088/1478-7814/37/1/314